NANO LETTERS

Letter

pubs.acs.org/NanoLett

Transient Absorption and Photocurrent Microscopy Show That Hot Electron Supercollisions Describe the Rate-Limiting Relaxation Step in Graphene

Matt W. Graham,*[,†,§,∥] Su-Fei Shi,[†,§,⊥] Zenghui Wang,[‡,§,#] Daniel C. Ralph,[†,§] Jiwoong Park,[‡,§] and Paul L. McEuen[†,§]

[†]Laboratory for Atomic and Solid State Physics, Cornell University, Ithaca, New York 14853, United States

[‡]Department of Chemistry and Chemical Biology, Cornell University, Ithaca, New York 14853, United States

[§]Kavli Institute at Cornell for Nanoscale Science, Ithaca, New York 14853, United States

Supporting Information

ABSTRACT: Using transient absorption (TA) microscopy as a hot electron thermometer, we show that disorder-assisted acoustic-phonon supercollisions (SCs) best describe the rate-limiting relaxation step in graphene over a wide range of lattice temperatures (T_l = 5−300 K), Fermi energies (E_F = ± 0.35 eV), and optical probe energies (~0.3−1.1 eV). Comparison with simultaneously collected transient photocurrent, an independent hot electron thermometer, confirms that the rate-limiting optical and electrical response in graphene are best described by the SC-heat dissipation rate model, $H = A(T_e^3 - T_l^3)$. Our data further show that the electron cooling rate in substrate-supported graphene is twice as fast as in suspended graphene sheets, consistent with SC model prediction for disorder.

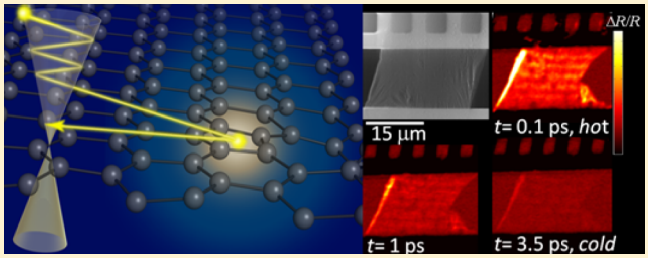

KEYWORDS: *Graphene, ultrafast, hot electrons, photocurrent, supercollisions*

With high electron mobility and uniform spectral response spanning the far-IR to visible regions, graphene is an attractive material for next generation optoelectronic devices such as fast photodetectors, bolometers, and plasmonic devices.[1−6] Graphene was originally predicted to have long (up to nanosecond) hot electron and hole (e−h) lifetimes resulting from its unusually large optic phonon energies and vanishing density of states.[7,8] However, time-resolved experiments show that the actual e−h relaxation time is orders of magnitude faster.[9−11] The mechanism for fast energy dissipation in graphene has been the subject of considerable debate, with differing reports advocating either optical phonon[12,13] or disorder-mediated acoustic phonon decay pathways.[14−16] Here we measure the electronic heat dissipation rate $H = C_e dT_e/dt$ using both transient absorption (TA) and transient photocurrent (TPC) thermometry. In particular, we report TA measurements in graphene while varying the lattice temperature, Fermi energy, and optical probe energy. Our data confirms that acoustic phonons supercollisions best describe the rate-limiting heat dissipation kinetics over the wide range of these parameters.

In graphene, hot electrons can efficiently dissipate heat by emitting optical phonons with allowed energy, $\hbar\omega_{op} \sim 0.2$ eV.[10−12] For electrons below this unusually high energy threshold, momentum conservation permits only low-energy (<4 meV, black arrows in Figures 1a and 2a) acoustic phonon emission, resulting in very long electron relaxation times.[7,11] However, Song et al. predicts the SC model dominates where electron heat dissipation occurs without crystal momentum conservation, involving the emission of high-energy ($\sim k_B T_e$) acoustic phonons with the momentum imbalance, q_{recoil} accounted for by disorder induced intrinsic lattice recoil (red arrow in Figure 1a).[14] This process, which results in faster cooling, is depicted in Figure 1a and has a signature kinetic rate,[14]

$$\frac{dT_e}{dt} = -\frac{H}{\alpha T_e} = -\frac{A}{\alpha}\frac{T_e^3 - T_l^3}{T_e} \quad (1)$$

where A/α is the SC rate coefficient, and T_l and T_e are the lattice and electron temperatures, respectively. Solving eq 1, $T_e(t) \cong T_o/(1 + AT_o t/\alpha)$ when $T_e(t) \gg T_l$ and $T_e(t) \cong T_l + (T_o - T_l)\exp(-3AT_l t/\alpha)$ when $T_e(t) - T_l \ll T_l$ where T_o is the initial electron temperature. Recent studies demonstrate that the SC model[14] successfully predicts graphene's photocurrent[15] and electrical[16] heating response. However, the applicability of the SC model to purely optical measurements has not been considered.

In previous optical TA measurements hot electron cooling has instead been predominately modeled using the hot optical

Received: August 16, 2013
Revised: October 14, 2013
Published: October 14, 2013

 © 2013 American Chemical Society dx.doi.org/10.1021/nl4030787 | *Nano Lett.* 2013, 13, 5497−5502

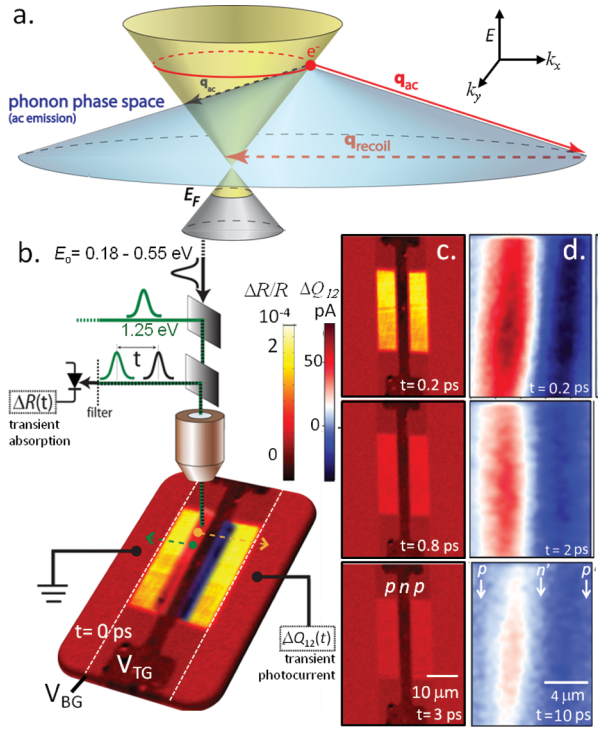

Figure 1. Transient absorption (TA) + photocurrent (TPC). (a) Supercollision cooling mechanism (red arrows). (b) Measurement setup collects the optical TA, $\Delta R(t)$, and electrical TPC, $\Delta Q_{12}(t)f$ response from graphene (yellow). (c) Ultrafast TA movie frames for electron relaxation at E_o = 0.4 eV probe, T_l = 5 K. (d) TPC movie frames of electron relaxation at p−n and n−p graphene junctions, T_l = 5 K.

phonon (HP) cooling bottleneck effect.[12,17] In the HP model, thermalized electrons (and holes) dissipate heat primarily by optic phonon emission from the Fermi−Dirac tails, where $E > \hbar\omega_{op}$. If electrons exchange their heat with optic phonons the two thermal baths are in approximate equilibrium, $T_e(t) \rightleftarrows T_{op}(t)$ over the lifetime, τ_{ph} of the dominate G-band optical phonon (see Figure 2a, ii).[12] This forms a cooling bottleneck that determines the overall electronic temperature approximately given by $T_e(t) \cong T_{op}/(1 + t/\tau_{op})$, where $\tau_{op}^{-1} = k_B T_{op}/(\hbar\omega_{op}\tau_{ph})$ and T_{op} is the initial optic phonon temperature.[12] In the $T_e(t) \gg T_l$ limit, both the HP and the SC models give identical functional forms. However, the two models make distinct predictions for the T_l dependence, E_F dependence, and the role of environment-induced disorder.

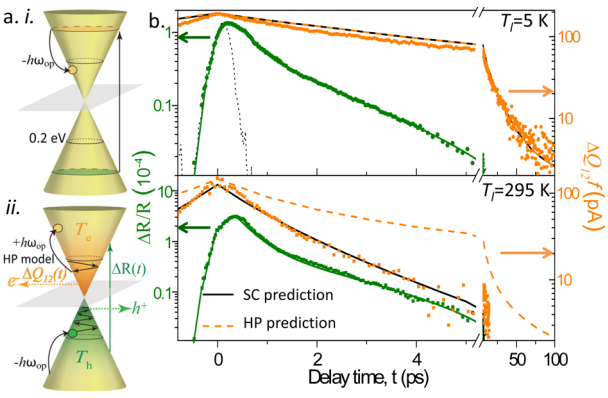

Figure 2. SC vs HP predictions. (a) Hot carriers thermalize and emit optic or acoustic phonons (black arrows). We probe the electron temperature using TA and TPC. (b) Pulse cross-correlation (dotted line). The TA kinetics (green) predict the TPC decay (orange) when SC model is invoked (black lines). The HP model (orange, dashed), however, fails at 295 K.

To differentiate between the HP and SC models, we compare each model against two independent thermometers of graphene temperature: (a) optical TA and (b) photothermal TPC. First, we optically probe the transient e−h population of a single graphene sheet using confocal scanning TA microscopy.[17] We detect both the spatial and the temporal transient reflectivity, $\Delta R(t)/R = [4/(n_s^2 - 1)](4\pi/c)\mathrm{Re}\Delta\sigma(E_o,t)$, where n_s is the substrate refractive index and $\Delta\sigma$ is the transient optical conductivity at energy, $E_o = 1/2(\hbar\omega_{probe})$.[18] Figure 1b shows our experiment setup where graphene at T_l = 5 K is excited with a 170 fs pump pulse at 990 nm, and the hot e−h pairs created are probed at tunable wavelengths ranging from 1200 to 3450 nm. In Figure 1c, we observe a photobleach signal (yellow) that corresponds to a ∼ 0.02% increase in probe beam reflectivity from Pauli blocking occurring at $E_o \pm E_F \cong 0.4$ eV. The subsequent frames of this TA movie (see Supplementary Movie) show hot electrons cooling uniformly. Figure 2b (green) plots the kinetic decay of $\Delta R(t)/R$ at T_l = 5 and 295 K obtained with a 1.5 μm spot centered on a electrostatically doped graphene p−n junction. In this first TA measurement at a graphene p−n junction, the kinetics exhibit a roughly T_l-independent biexponential decay similar to numerous existing graphene TA studies of single-layer graphene.[9,11,19,20]

After electrons thermalize in graphene, the TA response is directly connected with a physical hot electron temperature, that is extracted by fitting to the transient interband optical conductivity, $\Delta\sigma(E_o,t) = -e^2/4\hbar[f_{e/h}(T_e(t),E_o) - f_{e/h}(T_l,E_o)]$. Absolute temperatures can be obtained by evaluating the Fermi−Dirac hot-electron occupancy probability, $f_{e/h}(T_e(t),E_o)$ at the energy (E_o) optically probing in the graphene band structure, giving approximately,[18,21,22]

$$\Delta\sigma(t) = \frac{\pi e^2}{2h}\left[\tanh\left(\frac{E_o \pm E_F}{2k_B T_e(t)}\right) - \tanh\left(\frac{E_o \pm E_F}{2k_B T_l}\right)\right] \quad (2)$$

We further show at our hot electron densities that the *intra*band conductivity contributes negligibly to the transient reflectivity over our selected NIR probe regions (see Supporting Information). Using the HP model, eq 2 predicts TA decays nearly exponentially. The SC temperature model (eq 1) makes similar predictions only when $T_e(t) \gg T_l$. To fit the data in Figure 2b, two exponents (τ_1 and τ_2) are required. The faster component, $\tau_1 \cong 0.34$ ps, averages over the initial electron thermalization and optic phonon emission time scale and is discussed elsewhere.[11,23] Assuming the HP model describes the longer τ_2 component, our fits to Figure 2b with eq 2 requires τ_{ph} = 2.9 ps at 5 K and τ_{ph} = 3.3 ps at 295 K.

If we instead apply the SC mechanism in eq 1, analytic fits to the TA response in Figure 2b yield rate coefficients of A/α = 3.0 × 10^{-4} K^{-1} ps^{-1} at 5 K and 4.4 × 10^{-4} K^{-1} ps^{-1} and T_o = 1650 ± 300 K for T_l = 295 K. A similar SC rate of A/α = 5 × 10^{-4} K^{-1} ps^{-1} was recently reported directly from PC measurements.[15] This shows that the TA data can be explained using either the HP model or the SC model. However, the HP model predicts τ_{ph} values that are >2× longer than those measured via time-resolved Raman studies on near identical SiO_2 substrates.[24,25]

dx.doi.org/10.1021/nl4030787 | Nano Lett. 2013, 13, 5497−5502

We next use an independent thermometer to extract the hot electron temperature by simultaneously collecting the graphene TPC response, shown in Figures 1d and 2b (orange). Graphene's instantaneous photothermal current is given by $i(t) = \beta T_e(t)[T_e(t) - T_l]$, where β is proportional to the Seebeck coefficient.[15,26,27] We detect the time-integrated current $Q_1 f = f \int i(t,T_o)\, dt'$, where f is the pulse repetition rate (76 MHz). After a delay time t, the electron gas cools, and the second pulse at 0.8 eV reheats graphene to a new initial temperature, $(T_o^2 + T_e(t)^2)^{1/2}$. The TPC response, Q_{12}, is then obtained by integrating piecewise about t, giving,[15]

$$Q_{12}(t) = \int_0^t i(t', T_o)\, dt' + \int_t^\infty i(t' - t, \sqrt{T_o^2 + T_e(t)^2})\, dt' \quad (3)$$

In Figure 1d we show the resulting PC autocorrelation function, $\Delta Q_{12}(t,r) = 2Q_1 - Q_{12}(t,r)$, decays in both time and space about the graphene p−n junctions. In Figure 2b, we plot what our TA fit values (τ_{ph} for HP model and A/α for SC model) predict for the TPC amplitude decay (dashed lines). While the HP model approximately predicts the T_l = 5 K TPC response when T_{op} is a free parameter, it clearly fails to predict rapidly decaying TPC response observed at room temperature (orange dashed lines). On the contrary, the SC model correctly predicts the simultaneously acquired TPC kinetics at both T_l = 5 and 295 K from their corresponding optical TA results.

The striking ability of the SC model to predict the electrical TPC kinetics from the optical TA suggests both measurements can be well-described by the same SC heat loss rate, $H = A(T_e^3 - T_l^3)$. We now test the intrinsic T_l dependence of the SC model independently for both TPC (Figure 3a, inset) and TA (Figure 3b) measurements. With increasing T_l, the SC model solutions predict the cooling decay changes from a reciprocal to an exponential decay in time (Figure 3a). Comparing this SC model prediction against the TPC data in Figure 3a (inset), qualitative similarities are apparent. Here we numerically solve the TPC response function (eq 3) with no free parameters; as recently reported,[15] we demonstrate again the SC model (gray lines) predicts the TPC response. Here, the TPC kinetics were acquired at pump fluences corresponding to $T_o \cong 1250$ K for T_l = 295 K and ∼850 K otherwise. For a fixed incident photon flux, the TPC decay is approximately independent of the excitation wavelength.

Unlike TPC, in Figure 2b our TA kinetic decay rate for relatively large E_o = 0.4 eV showed only a weak T_l dependence. However, similar TA measurements performed with smaller E_o ∼0.18 eV show markedly different behaviors Figure 3b. Specifically, when $E_o - E_F < \hbar\omega_{op}$, strongly T_l dependent kinetics emerge. In Figure 3b,i, we employ NIR-IR pump, mid-IR probe TA at E_o = 0.18 eV < $\hbar\omega_{op}$ and plot the graphene mid-IR kinetics at T_l = 5 K (blue) and 295 K (red). Fitting Figure 3b,*i* at 5 K (blue line) using eqs 1 and 2 plus a τ_1 exponential component, we extract τ_1 = 0.36 ps and $A/\alpha = 2.4 \times 10^{-4}$ p s^{-1} K^{-1}. Using these 5 K TA parameters, we analytically solve the SC model at T_l = 295 K and show the result in eq 2 predicts the observed kinetics (red line). To probe closer to E_F, we next apply a back gate voltage such that $E_o - E_F \cong 0.04$ eV. Fitting the remarkably longer T_l = 5 K kinetics (blue line) in Figure 3b,ii, gives moderately faster SC-rate of $A/\alpha \cong 5.2 \times 10^{-4}$ ps^{-1} K^{-1}. Using this rate, we again solve the SC model to predict cooling at T_l = 295 K, and the result closely predicts the radically faster kinetics observed (red line). We conclude the SC kinetic rate model predicts T_l-dependent TA response in graphene.

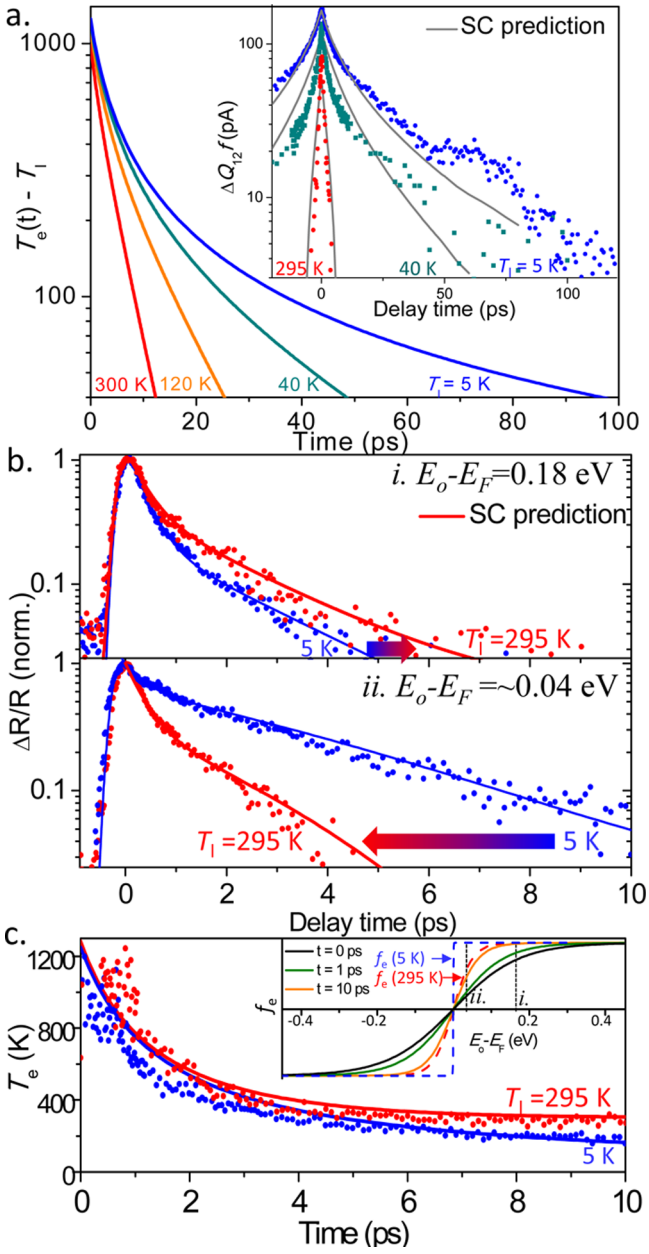

Figure 3. Lattice temperature dependence. (a) Analytic SC model solutions. (inset) Using eq 3, the $T(t, T_l)$ curves predict the observed TPC decay with no free parameters. (b) Mid-IR probe TA kinetics for (i) E_o = 0.18 eV and (ii) $E_o - E_F \cong 0.04$ eV. Using the 5 K TA parameters, the SC model predicts the 295 K result. (c) Solving eq 3 for T_e, we invert the data points in b,ii and show $T_e(t)$ roughly agrees with the SC model (solid lines). (inset) TA is proportional to the difference in the SC model electronic occupancies, $f_e(T_e(t), E_o - E_F)$ (solid lines) and $f_e(T_l, E_o - E_F)$ (dashed lines).

The origin of the T_l-dependent TA can be understood by plotting the temporal evolution of the hot electron occupancy probabilities $f_e(T_e(t), E_o - E_F)$ in Figure 3c (inset, solid lines). For a given $E_o - E_F$ probe window, $\Delta\sigma(t,E_o)$ is proportional to $f_e(T_e(t)) - f_e(T_l)$, where $f_e(T_l)$ is the equilibrium electronic occupancy at T_l = 5 and 295 K, respectively (dashed lines). At high probe energies, $f_e(295\text{ K}) \cong f_e(5\text{ K}) \cong 0$ making $\Delta\sigma(t, E_o)$ roughly T_l-independent, as observed in Figures 2b and 3b,i. In

dx.doi.org/10.1021/nl4030787 | Nano Lett. 2013, 13, 5497−5502

contrast at low probe energies $f_e(295\ K) \gg f_e(5\ K)$, which makes hot electron kinetics effectively faster at room temperature as observed in Figure 3b,ii. Similar strong T_l-dependent responses have been reported in both recent THz studies[28] and in degenerate far-IR TA measurements by Winnerl et al.[20,29] The SC model roughly predicts these previously reported long-lived transients, which were largely attributed to substrate heating effects before.

In Figures 1−3, we demonstrate that the SC model predicts the T_l-dependent TA interband electron kinetics across a wide range of probe energies. Using the SC model, we may further invert our TA response to obtain $T_e(t)$. In Figure 3c we convert each data point in Figure 3b,ii to its corresponding temperature, by solving eq 2 for $T_e(t)$, we also included a $\tau_1 = 0.35$ ps exponential component, accounting for nonthermalized electrons at short times. The resulting model-independent inversion approximately agrees with temperatures (solid lines) obtained by directly solving eq 1, the SC model.

So far, our SC model predictions required prior knowledge of the intrinsic graphene doping to evaluate both initial temperature, T_o and rate, A/α. In Figure 4 we study the E_F-dependence of the TA decay dynamics and extract two SC parameters: T_o and A/α. In Figure 4a, we plot the E_F-dependence of the $T_l = 5$ K mid-IR TA amplitude. By tuning E_F via a capacitively coupled back-gate where $E_F \propto (V_{BG})^{1/2}$, we observe that both the TA signal amplitude (blue circles) and lifetime (red squares) increase as $E_o \rightarrow \pm E_F$. As previously observed, as $E_F > E_o$ the hot electron Pauli blocking effect is effectively turned off.[30] Accordingly, both the decay time and TA amplitude decrease in Figure 4. The simple interband conductivity in eq 2 captures this overall trend well. The resulting fit (orange line) requires an initial electron temperature of ∼1200 K, which agrees with estimates at similar fluences extracted earlier from TA SC model fits or from photothermal current measurements.[15]

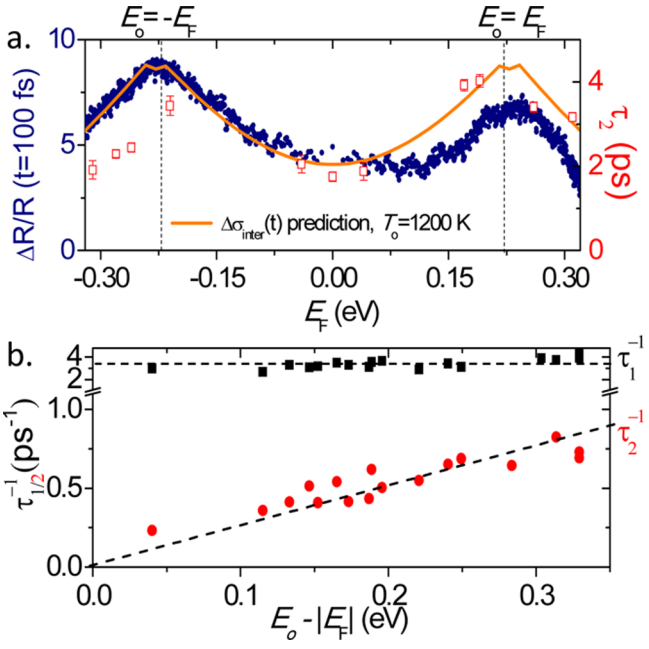

Figure 4. E_F dependence. (a) $E_o = 0.18$ eV TA at $T_l = 5$ K vs E_F. As $\pm E_F \rightarrow \sim E_o$, both the transient amplitude and τ_2 increase. The SC model interband $\sigma(t)$ fits TA response well for $T_o = 1200$ K. (b) TA lifetimes τ_2^{-1} scale linearly from the origin, with slope $A/\alpha k_B$. τ_1 is constant at ∼0.36 ps.

In Figure 4b, we systematically tune E_F and plot the extracted 5 K rates τ_1^{-1} and τ_2^{-1} rates against $E_o - |E_F|$. The initial TA decay rate is roughly invariant to E_F, with $\tau_1 \cong 0.36$ ps. Since this is longer than our 170 fs pulse width, this E_F invariance constant τ_1 suggests that the electrons are not fully thermalized. When $T_e(t) \gg T_l$, the SC model in eq 2 predicts $\tau_2^{-1} \cong (E_o \pm E_F)A/(k_B\alpha)$. Accordingly, we find the line of best fit intersects the origin with a slope of 2.6 ± 0.1 ps^{-1} eV^{-1}, which implies $A/\alpha = 2.3 \times 10^{-4}$ K^{-1} ps^{-1}. Instead of tuning E_F, we can systematically tune the probe energy $2E_o$, we find the extracted rate τ_2^{-1} also varies according to $(E_o \pm E_F)A/(k_B\alpha)$ at 5 K. As shown in Figure 5a (yellow squares) the fitted slope gives $A/\alpha = 2.3 \pm 0.4 \times 10^{-4}$ ps^{-1} K^{-1} and intercept gives $E_F = 190 \pm 90$ meV. Thus, the 5 K TA kinetic dependence on both E_F and E_o give the same the same SC cooling rate.

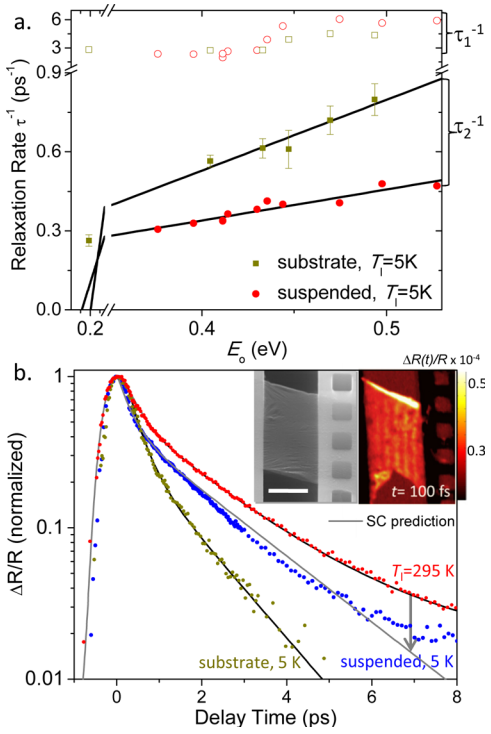

Figure 5. Suspended graphene. (a) τ_2^{-1} varies linearly with probe energy, the intercept correspond to the intrinsic doping, E_F. (b) Suspended TA kinetics for $E_o = 0.4$ eV. The SC model predicts the 5 K decay with no free parameters (blue line) from the 295 K TA parameters. (inset) SEM image and TA microscopy (at $t = 0.1$ fs) of suspended graphene. The scale bar is 10 μm.

Ab initio predictions of the SC cooling rate are given in Song et al. as:[14,31,32] $(A/\alpha) = [6\zeta(3)/\pi^2][\lambda/(k_F l)](k_B/\hbar) \cong (2/3)[\lambda/(k_F l)](k_B/\hbar)$ where the electron−phonon coupling strength is $\lambda = [D^2/(\rho s^2)][2E_F/(\pi(\hbar v_F)^2)]$.[14] Using estimates for the deformation potential, $D = 10 - 30$ eV, $E_F = 0.1$ eV, and a mean free path of $k_F l = 10$, this theory predicts: $A/\alpha = 10^{-4}$ to 10^{-3} K^{-1} ps^{-1}. (The range comes from the uncertainty in D). The best match to our experiments indicate $D = 8-14$ eV, well within the expected range. The SC model further predicts that $A/\alpha \propto E_F/k_F l \propto E_F/G$, where G is the device conductivity. For example over the back voltage sweep from 0 to 80 V, the E_F changes from 0.1 to 0.3 eV, and our conductance changes from 0.1 to 0.4 mS; accordingly A/α vs E_F changes little. In rough

dx.doi.org/10.1021/nl4030787 | Nano Lett. 2013, 13, 5497−5502

accord with the SC model, in Figure 4b A/α changes only from 2.0×10^{-4} ps^{-1} K^{-1} to 2.7×10^{-4} ps^{-1} K^{-1}.

Short-range disorder is central to the SC model, providing acoustic phonons with the requisite lattice recoil momentum (q_{recoil}, see Figure 1a).[14] If we now suspend a graphene sheet in vacuum, how will this new environment impact the SC-cooling rate? Figure 5 shows the cooling mechanism in suspended graphene, resulting in a cooling rate ~2× slower than its substrate supported counterpart. By plotting the decay rate τ_2^{-1} vs probe energy in Figure 5a, the linear fit line for suspended graphene (red circles) requires $A/\alpha = 1.1 \pm 0.2 \times 10^{-4}$ ps^{-1} K^{-1}, and the intercept gives intrinsic doping at $E_F = 95 \pm 32$ meV. Fitting suspended graphene kinetics using the alternate HP model would require a prohibitively long $\tau_{ph} = 5.1$ ps optical phonon lifetime.[24,25]

Figure 5b compares the TA kinetics at $T_l = 5$ and 295 K. Fitting the 295 K the decay using eqs 1−2, we again extract a roughly 2× slower rate coefficient, $A/\alpha = 1.4 \pm 0.1 \times 10^{-4}$ ps^{-1} K^{-1} and $T_o = 850$ K. The 2-fold slower cooling rate of suspended graphene vs substrate supported is justified by the SC-prediction that $A/\alpha \propto (k_F l)^{-1}$. Accordingly, transport studies have shown $k_F l$ is approximately twice as long in suspended CVD-grown graphene vs substrate suspended.[33−35] Lastly we demonstrate the SC model predicts T_l-dependent hot electrons kinetics for suspended graphene, as demonstrated earlier for substrate-supported graphene. Using the 295 K A/α extracted in Figure 5b, we solve eqs 1 and 2 for the 5 K result. We find the SC model predicts (gray line) the 5 K suspended graphene TA kinetic decay with no free parameters.

The ability of the SC model to predict graphene's optical, photocurrent,[15] and electrical response[16] under a wide variety of conditions definitively show that the SC model best describes the rate-limiting heat dissipation step in photoexcited doped graphene. Existing models, such as the HP model, do not account for the strongly T_l-dependent kinetics observed in both TPC and TA measurements. The HP model further requires prohibitively long optic phonon lifetimes, $\tau_{ph} \sim 5$ ps, to fit suspended graphene kinetics. The SC model provides a new interpretation for previous graphene TA studies and suggests a new time line of event for electronic relaxation in graphene. Over an initial time scale $\tau_1 < 0.4$ ps, photoexcited carriers rapidly thermalize and dissipate energy to optical phonons.[11,12] The vast majority of electrons now have $E < \hbar\omega_{op}$, resulting in a cooling bottleneck. Here we show this bottleneck cools according to the SC-cooling kinetic rate law, $H_{SC} = A(T_e^3 - T_l^3)$ with a rate coefficient determined by intrinsic disorder. Collectively, Joule heating,[16] photocurrent,[15] and optical measurements can be described by the same SC model.[14] This suggests a reliable method for determining the electronic temperature in graphene has emerged.

Experimental Methods. The CVD growth, fabrication, and characterization of both suspended and of p−n junction graphene is found in the Supporting Information. In p−n junctions, a tunable back gate (BG) and top gate (TG) couple to graphene, defining two p−n doped regions where the PC production is maximal. The collected PC amplitude is plotted as the laser is raster scanned over the p−n junction (see superimposed PC map in Figure 1a). We optically excite the graphene p−n junction region with pulses produced by two synchronously locked independently tunable oscillators and NIR optical parametric oscillator (OPO). Similar TA and TPC kinetics are obtained from both oscillator/OPO or white-light supercontinuum excitation geometries. We simultaneously collect the change in reflectivity ($\Delta R(t)/R$, TA) and electrical current generated ($\Delta Q_{12}(t)f$, TPC) as functions of pulse delay time.

Cross-correlation at the device position yields a 170 fs fwhm pulse duration. After a mechanical delay stage, the two beams are aligned in a collinear geometry at and beamsplitter and coupled into the microscope (Olympus BX-51) through a 50XIR Olympus objective by a scanning mirror (SM, PI no. $S-334.2SL$). For mid-IR TA we use a reflective objective with a ~3.5 μm spot-size. TA signal was detected by lock-in detection at 0.9 MHz pump-beam AOM modulation rate using either amplified InGaAs or PbSe detectors. Pump power typically corresponds to an initial electron carrier density of $\sim 3 \times 10^{12}$ cm^{-2}. Probe power was ~1/20 of pump, unless specified. TPC was collected at a 3 kHz modulation rate.

■ ASSOCIATED CONTENT

Ⓢ Supporting Information

Details on experimental setup and details on data modeling methods. Supporting videos of the ultrafast transient absorption cooling process of both $p-n$ junction and suspended graphene are also available online. This material is available free of charge via the Internet at http://pubs.acs.org.

■ AUTHOR INFORMATION

Corresponding Author

*E-mail: graham@physics.oregonstate.edu.

Present Addresses

[‖]Oregon State University, Department of Physics, Corvallis, Oregon 97331, United States.

[⊥]University of California, Berkeley, Department of Physics, Berkeley, California 94720, United States.

[#]Case Western Reserve University, Electrical Engineering, Cleveland, Ohio 44106, United States.

Notes

The authors declare no competing financial interest.

■ ACKNOWLEDGMENTS

This research was supported by the Kavli Institute at Cornell for Nanoscale Science (KIC), AFOSR (FA 9550-10-1-0410), by the NSF through the Center for Nanoscale Systems and by the MARCO Focused Research Center on Materials, Structures, and Devices. Device fabrication was performed at the Cornell Nanofabrication Facility/National Nanofabrication Infrastructure Network.

■ REFERENCES

(1) Mueller, T.; Xia, F.; Avouris, P. *Nat. Photonics* **2010**, *4* (5), 297−301.

(2) Lemme, M. C.; Koppens, F. H. L.; Falk, A. L.; Rudner, M. S.; Park, H.; Levitov, L. S.; Marcus, C. M. *Nano Lett.* **2011**, *11* (10), 4134−4137.

(3) Bonaccorso, F.; Sun, Z.; Hasan, T.; Ferrari, A. C. *Nat. Photonics* **2010**, *4* (9), 611−622.

(4) Yan, J.; Kim, M.-H.; Elle, J. A.; Sushkov, A. B.; Jenkins, G. S.; Milchberg, H. M.; Fuhrer, M. S.; Drew, H. D. *Nat. Nanotechnol.* **2012**, *7*, 472−478.

(5) Blake, P.; Brimicombe, P. D.; Nair, R. R.; Booth, T. J.; Jiang, D.; Schedin, F.; Ponomarenko, L. A.; Morozov, S. V.; Gleeson, H. F.; Hill, E. W.; Geim, A. K.; Novoselov, K. S. *Nano Lett.* **2008**, *8* (6), 1704−1708.

(6) Fong, K. C.; Schwab, K. C. *Phys. Rev. X* **2012**, *2* (3), 031006.

(7) Bistritzer, R.; MacDonald, A. H. *Phys. Rev. Lett.* **2009**, *102* (20), 206410.

(8) Kubakaddi, S. S. *Phys. Rev. B* **2009**, *79* (7), 075417.
(9) Dawlaty, J. M.; Shivaraman, S.; Chandrashekhar, M.; Rana, F.; Spencer, M. G. *Appl. Phys. Lett.* **2008**, *92* (4), 042116.
(10) Winnerl, S.; Orlita, M.; Plochocka, P.; Kossacki, P.; Potemski, M.; Winzer, T.; Malic, E.; Knorr, A.; Sprinkle, M.; Berger, C.; de Heer, W. A.; Schneider, H.; Helm, M. *Phys. Rev. Lett.* **2011**, *107* (23), 237401.
(11) Breusing, M.; Ropers, C.; Elsaesser, T. *Phys. Rev. Lett.* **2009**, *102* (8), 086809.
(12) Wang, H.; Strait, J. H.; George, P. A.; Shivaraman, S.; Shields, V. B.; Chandrashekhar, M.; Hwang, J.; Rana, F.; Spencer, M. G.; Ruiz-Vargas, C. S.; Park, J. *Appl. Phys. Lett.* **2010**, *96*, 081917.
(13) Rana, F.; Strait, J. H.; Wang, H.; Manolatou, C. *Phys. Rev. B* **2011**, *84* (4), 045437.
(14) Song, J. C. W.; Reizer, M. Y.; Levitov, L. S. *Phys. Rev. Lett.* **2012**, *109* (10), 106602.
(15) Graham, M. W.; Shi, S.-F.; Ralph, D. C.; Park, J.; McEuen, P. L. *Nat. Phys.* **2013**, *9* (2), 103−108.
(16) Betz, A. C.; Jhang, S. H.; Pallecchi, E.; Ferreira, R.; Fève, G.; Berroir, J.-M.; Plaçais, B. *Nat. Phys.* **2013**, *9* (2), 109−112.
(17) Huang, L.; Gao, B.; Hartland, G.; Kelly, M.; Xing, H. *Surf. Sci.* **2011**, *605* (17−18), 1657−1661.
(18) Malard, L. M.; Fai Mak, K.; Castro Neto, A. H.; Peres, N. M. R.; Heinz, T. F. *New J. Phys.* **2013**, *15* (1), 015009.
(19) Sun, D.; Wu, Z.-K.; Divin, C.; Li, X.; Berger, C.; de Heer, W. A.; First, P. N.; Norris, T. B. *Phys. Rev. Lett.* **2008**, *101* (15), 157402.
(20) Limmer, T.; Houtepen, A. J.; Niggebaum, A.; Tautz, R.; Da Como, E. *Appl. Phys. Lett.* **2011**, *99* (10), 103104−103104-3.
(21) Castro Neto, A. H.; Guinea, F.; Peres, N. M. R.; Novoselov, K. S.; Geim, A. K. *Rev. Mod. Phys.* **2009**, *81* (1), 109−162.
(22) Kampfrath, T.; Perfetti, L.; Schapper, F.; Frischkorn, C.; Wolf, M. *Phys. Rev. Lett.* **2005**, *95* (18), 187403.
(23) Tielrooij, K. J.; Song, J. C. W.; Jensen, S. A.; Centeno, A.; Pesquera, A.; Zurutuza Elorza, A.; Bonn, M.; Levitov, L. S.; Koppens, F. H. L. *Nat. Phys.* **2013**, *9* (4), 248−252.
(24) Kang, K.; Abdula, D.; Cahill, D. G.; Shim, M. *Phys. Rev. B* **2010**, *81* (16), 165405.
(25) Wu, R.; Zhang, Y.; Yan, S.; Bian, F.; Wang, W.; Bai, X.; Lu, X.; Zhao, J.; Wang, E. *Nano Lett.* **2011**, *11* (12), 5159−5164.
(26) Xu, X.; Gabor, N. M.; Alden, J. S.; van der Zande, A. M.; McEuen, P. L. *Nano Lett.* **2009**, *10* (2), 562−566.
(27) Gabor, N. M.; Song, J. C. W.; Ma, Q.; Nair, N. L.; Taychatanapat, T.; Watanabe, K.; Taniguchi, T.; Levitov, L. S.; Jarillo-Herrero, P. *Science* **2011**, *334* (6056), 648−652.
(28) Strait, J. H.; Wang, H.; Shivaraman, S.; Shields, V.; Spencer, M.; Rana, F. *Nano Lett.* **2011**, *11* (11), 4902−4906.
(29) Winnerl, S.; Göttfert, F.; Mittendorff, M.; Schneider, H.; Helm, M.; Winzer, T.; Malic, E.; Knorr, A.; Orlita, M.; Potemski, M.; Sprinkle, M.; Berger, C.; Heer, W. A. d. *J. Phys.: Condens. Matter* **2013**, *25* (5), 054202.
(30) Horng, J.; Chen, C.-F.; Geng, B.; Girit, C.; Zhang, Y.; Hao, Z.; Bechtel, H. A.; Martin, M.; Zettl, A.; Crommie, M. F.; Shen, Y. R.; Wang, F. *Phys. Rev. B* **2011**, *83* (16), 165113.
(31) Chen, W.; Clerk, A. A. *Phys. Rev. B* **2012**, *86* (12), 125443.
(32) Tse, W.-K.; Das Sarma, S. *Phys. Rev. B* **2009**, *79* (23), 235406.
(33) Du, X.; Skachko, I.; Barker, A.; Andrei, E. Y. *Nat. Nanotechnol.* **2008**, *3* (8), 491−495.
(34) Bolotin, K. I.; Sikes, K. J.; Hone, J.; Stormer, H. L.; Kim, P. *Phys. Rev. Lett.* **2008**, *101* (9), 096802.
(35) Adam, S.; Sarma, S. D. *Solid State Commun.* **2008**, *146* (9−10), 356−360.